Redox Metal-Support Interaction of CoO_x/Ti_2O_3 to Enhance Catalytic Performance for Hydrodeoxygenation of Anisole

Weizhou Sun,[1] Masanori Nagao,[1,2] Miyu Sato,[1] Shuhei Shimoda,[3] Yuichi Kamiya,[4] and Ryoichi Otomo[4, *]

[1]Graduate School of Environmental Science, Hokkaido University, Nishi 5 Kita 10, Kita-ku, Sapporo 060-0810, Japan. [2]National Institute of Technology, Tomakomai College, 443 Nishikioka, Tomakomai 059-1275, Japan. [3]Institute for Catalysis, Hokkaido University, Nishi 10 Kita 21, Kita-ku, Sapporo 001–0021, Japan. [4]Faculty of Environmental Earth Science, Hokkaido University, Nishi 5 Kita 10, Kita-ku, Sapporo 060-0810, Japan.

*Corresponding author: Dr. Ryoichi Otomo

e-mail: otomo@ees.hokudai.ac.jp

Abstract

This study found that CoO_x/Ti_2O_3 catalyst showed high activity, selectivity, and stability for hydrodeoxygenation (HDO) of anisole to benzene. Due to the reductivity of Ti_2O_3, redox reaction occurred between Ti_2O_3 and CoO_x, forming cobalt species with low oxidation state such as CoO and metallic Co. These cobalt species on Ti_2O_3 enhanced catalytic performance for the HDO reaction. On the other hand, CoO_x supported on other supports including TiO_2, Al_2O_3, SiO_2 and active carbon was in the form of Co_3O_4, and showed only low catalytic activity. H_2-TPR and H_2-TPD experiments demonstrated that CoO_x supported on Ti_2O_3 was easily reduced to metallic Co, which had the ability to activate H_2. CoO_x/Ti_2O_3 and CoO_x/TiO_2 catalysts deactivated more or less by partial oxidation of the cobalt species during the HDO reaction. The reduction of the partially oxidized cobalt species was promoted by the redox reaction between the cobalt species and Ti_2O_3, and therefore CoO_x/Ti_2O_3 showed much longer catalyst life than CoO_x/TiO_2.

Keywords

Cobalt catalyst; Hydrodeoxygenation; Metal-Support Interaction; Ti_2O_3; Titanium suboxide.

1. Introduction

Hydrodeoxygenation (HDO) is a highly important chemical reaction for upgrading biomass feedstocks to chemicals and fuels. In particular, it is effective for the synthesis of aromatic and cycloaliphatic compounds by selectively or completely removing oxygen-containing functional groups from lignin-derived oxygenate compounds.[1]

Having a C_{aryl}-O-C_{alkyl} moiety, which is common in lignin-derived oxygenates, anisole is a model compound for evaluating catalytic performance in HDO reactions.[2] Despite its simple molecular structure, anisole undergoes various parallel and sequential reactions in the HDO reaction, resulting in very complex reaction pathways (Scheme 1).[3,4] Direct demethoxylation of anisole produces benzene with methane and water (or methanol). Benzene is also produced through sequential demethylation and dehydroxylation via phenol as intermediate. Intramolecular methylation and transmethylation are more likely to occur over catalysts with strong acidity at high temperature, producing methylated aromatic compounds and benzene. When using a catalyst with high hydrogenation ability at high pressure of H_2, ring hydrogenation occurs, producing cyclohexane as the final product. To selectively obtain a desired product from anisole through the HDO reaction, it is important to select a catalyst and reaction conditions so that only a specific reaction proceeds preferentially, while suppressing undesirable side reactions. For example, to selectively synthesize benzene from anisole, it is important to suppress methylation reactions and ring hydrogenation.

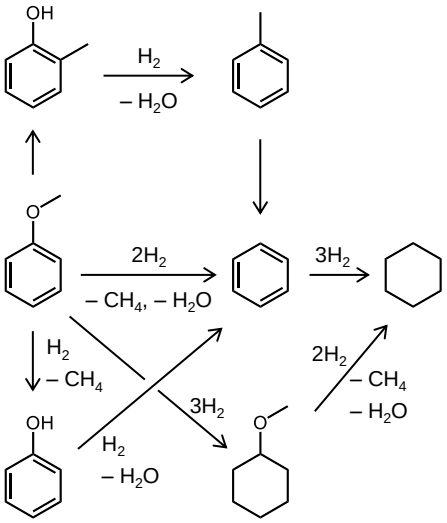

Scheme 1 Reaction pathway for hydrodeoxygenation of anisole to benzene and other side-reactions.

In HDO reactions, catalysts take vital roles because they determine productivity and product selectivity of the reactions, and thus greatly affect the efficiency and feasibility of the reaction process. A wide variety of catalysts have been developed for HDO reactions including precious metal catalysts (e.g., Ru, Pd, and Pt) and non-precious metal catalysts (e.g., Co, Ni, and Mo).[5] Since precious metals have several problems such as high cost and limited resources concentrated in specific regions, it is desirable to use effectively active species other than precious metals.[6]

Cobalt species are known to be effective non-precious metal catalysts to promote HDO reactions and have been used in various forms including metallic Co,[7–15] single oxide,[16] and other forms.[17–19] Cobalt species have several functions indispensable for HDO reactions. For example, metallic Co played a critical role of activating H_2.[20] Mochizuki et al. reported that Co/SiO_2 showed the highest activity and aromatic selectivity for the HDO reactions of guaiacol and woody tar among Co/SiO_2, Ni/SiO_2, Pd/SiO_2, Pt/SiO_2, and $CoMo/Al_2O_3$ catalysts.[7] They proposed that the superior catalytic performance was due to the activation of H_2 on metallic Co. However, metallic Co is more

easily oxidized than precious metals and cobalt catalysts would deactivate due to the oxidation. Conversely, since cobalt is difficult to reduce once it is oxidized, high temperature and/or high H_2 pressure is required for reducing the oxidized cobalt species. Liu et al. found that the unreduced cobalt catalyst showed no activity at all in HDO of eugenol and pointed out the importance to reduce cobalt species sufficiently. [11] The deactivation of cobalt catalysts caused by the oxidation has also been reported in Fischer-Tropsch synthesis.[21] To maintain the high activity, it is necessary to keep cobalt species metallic state during the HDO reaction.

Most of the catalysts reported so far are used in supported forms with diverse support materials in HDO reactions.[22] It has been reported that the performance of cobalt catalysts was highly dependent on the supports.[23–25] Liu et al. compared cobalt catalysts supported on various supports in HDO of eugenol, among which Co/TiO_2 showed the best catalytic performance.[11] They proposed that the strong metal-support interaction (SMSI) played an important role in Co/TiO_2 to show the high activity despite the low dispersion of the cobalt species. SMSI was reported to be also effective for suppressing the leaching of cobalt species from the TiO_2-supported catalyst in liquid-phase hydrogenation reactions.[26] Hongkailers et al. compared cobalt catalysts supported on anatase and rutile TiO_2. The rutile-supported catalyst showed higher initial activity due to the large amount of Ti^{3+} formed on the catalyst surface, whereas the anatase-supported one showed higher stability.[15]

In this study, we focused on Ti_2O_3 as support for cobalt species. Ti_2O_3 is a metastable titanium suboxide composed of Ti^{3+}. Ti_2O_3 has physical properties and chemical reactivities different from those of TiO_2 owing to the difference in oxidation state of titanium.[27–29] It has been reported that

Ti^{3+} on the surface of Ti_2O_3 was readily oxidized to Ti^{4+} when it was exposed to O_2 or air.[30,31] Therefore, it is predicted that by combining Ti_2O_3 with a metal oxide that is more easily reduced than Ti_2O_3, such as Co_3O_4, redox reaction would occur to maintain the metal species in partially or completely reduced state. In this study, we applied Ti_2O_3 as catalyst support in expectation of reducing CoO_x and demonstrated that CoO_x/Ti_2O_3 was a highly active catalyst for HDO of anisole, verifying the above hypothesis.

2. Experimental

2.1. Synthesis of Ti_2O_3

Ti_2O_3 was synthesized by solid-phase reduction of rutile TiO_2 (STR-100N, Sakai Chemical Industry) with TiH_2 (Alfa Aesar).[31] TiO_2 and TiH_2 with a molar ratio of 2.1: 1 were ground together for 30 min using a mortar and a pestle to obtain a homogeneously mixed precursor. The precursor was put in a quartz glass tube connected to a vacuum line and heated at 670 °C (10 °C/min) under vacuum for 24 h by an electric furnace. Then, the sample was cooled to ambient temperature under vacuum and black powdery Ti_2O_3 product was taken out. The obtained sample was characterized by TG, XPS, and XRF (Figure S1 and S2, and Table S1, respectively), confirming that Ti_2O_3 (JCPDS 43-1033) was obtained in high purity.

2.2. Synthesis of Supported CoO_x Samples

Ti_2O_3-supported CoO_x was synthesized by the precipitation-deposition method.[32,33] First,

0.9861 g of $Co(NO_3)_2 \cdot 6H_2O$ (FUJIFILM Wako Pure Chemical, 98%) was dissolved in 100 mL of Milli-Q water. 1.8 g of Ti_2O_3 was added to the solution with stirring. Then, 1 M NH_3 aqueous solution (FUJIFILM Wako Pure Chemical) was added dropwise to the mixture to adjust pH of the solution at ~9. After the mixture was aged at 80 ℃ for 4 h, the solid was recovered by filtration and washed with deionized water. The recovered solid was dried at 80 ℃ for 24 h in an oven and finally heated in He flow (10 mL/min) at 300 °C for 4 h. The loading amount of CoO_x was 10 wt% as cobalt. In addition to Ti_2O_3, rutile TiO_2 (STR-100N, Sakai Chemical Industry), SiO_2 (AEROSIL 130, Nippon Aerosil), Al_2O_3 (AluC, Nippon Aerosil), and active carbon (FUJIFILM Wako Pure Chemical) were used as support material.

As a comparison, 10 wt% MoO_x/ZrO_2 was synthesized following the reported procedure.[34] Aqueous solution of $(NH_4)_6Mo_7O_{24}$ (FUJIFILM Wako Pure Chemical) was impregnated on monoclinic ZrO_2 (RC-100, Daiichi Kigenso Kagaku Kogyo) by the incipient wetness method. Finally, the obtained solid was calcined in air at 550 °C for 3 h.

2.3. Characterization

Structure of samples was examined by powder X-ray diffraction using a Bruker D2 PHASER diffractometer with monochromatic Cu Kα radiation (30 kV, 10 mA). Diffraction patterns were recorded in the 2θ range of 10° to 70° with a step of 0.05°. To measure XRD patterns of samples after reduction with H_2, the reduced samples were cooled down to ambient temperature while H_2 was flowing. To recover catalysts used in catalytic reaction runs, the gas flow was switched from the

reactant feed to N_2 after the reaction and the catalyst was cooled down to ambient temperature while N_2 was flowing. In both cases, the samples were taken out from the glass tube and diffraction patterns were recorded in ambient air.

Loading amount of cobalt in supported CoO_x samples was determined by ICP-AES using a Shimadzu ICPE-9000 analyzer. Due to the difficulty in dissolving Ti_2O_3 into aqueous solution, the concentration of cobalt residual in the filtrate was measured after the recovery of supported CoO_x by filtration. The loading amount of cobalt was calculated by subtracting the amount of residual cobalt from that of initially added cobalt.

Particle morphology of Ti_2O_3 and CoO_x/Ti_2O_3 was observed by scanning electron microscopy (SEM) using a Hitachi S-4800 microscope. The acceleration voltage and emission current were 10 kV and 10 mA, respectively. CoO_x/Ti_2O_3 and CoO_x/TiO_2 samples were also observed by transmission electron microscope (TEM) using a JEOL JEM-2100F microscope with an accelerating voltage of 200 kV.

N_2 adsorption isotherms of supported CoO_x samples were measured on a MicrotracBEL BELSORP-mini analyzer at liquid nitrogen temperature. Specific surface area of the samples was calculated by the Brunauer–Emmett–Teller (BET) method. Before measurement, the samples were pretreated in N_2 flow at 200 °C for 1h.

Oxidation state of cobalt near the solid surface was examined by X-ray photoelectron spectroscopy using a JEOL JPS-9200 spectrometer. All the samples were stored overnight at 40 °C under vacuum. The samples were fixed on a carbon tape under ambient conditions and evacuated for

2 h in the chamber of the spectrometer. Al Kα radiation was used as X-ray source. The applied voltage and emission current were 10 kV and 10 mA, respectively. Narrow scan spectra were measured with pass energy of 10 eV. The measured spectra were analyzed using JEOL SPECSURF Analysis software. Charge correction was performed using C 1s peak of the carbon tape (284.5 eV). Baseline was drawn by the Shirley method, and curve fitting of spectra was performed using Gauss-Lorentz mixed function (0.5: 0.5) with the same full width at half maximum value. The samples identical to those for the XRD measurement after the reduction with H_2 or catalytic reaction runs were used for the XPS measurement.

Temperature-programmed reduction with H_2 (H_2-TPR) was conducted on supported CoO_x samples using a MicrotracBEL BELCAT analyzer with a thermal conductivity detector (TCD). Samples (0.050 g) in a quartz glass tube were pretreated in 1% O_2/He (25 mL/min) at 200 °C for 1 h to mimic the oxidation of cobalt species that occurs during catalytic reactions and cooled down to 100 °C. The gas flow was switched to He to purge the samples for 1 h. Finally, the samples were heated to 800 °C at a rate of 10 °C/min in 1% H_2/Ar flow (25 mL/min) and the consumption of H_2 was monitored by the TCD. The amount of consumed H_2 was calculated using a calibration curve.

Temperature-programmed desorption of H_2 was measured on a home-made continuous gas flow reactor equipped with an ANELVA M-101QA quadrupole mass spectrometer (MS). Samples (0.10 g) in a quartz glass tube were pretreated in H_2 flow (30 mL/min) at 250 ºC for 0.5 h. The samples were cooled down to 50 ºC, where H_2 was adsorbed on the samples for 1 h. Then, the samples were purged in Ar flow at 50 ºC for 0.5 h. Finally, the samples were heated from 50 to 800 ºC at a rate of

10 ºC/min in Ar flow (25 mL/min) and MS signal for H_2 (m/z = 2) was monitored at the outlet of the quartz tube.

2.4. Hydrodeoxygenation of Anisole

Vapor-phase hydrodeoxygenation of anisole was conducted at atmospheric pressure on a vertical fixed-bed gas flow reactor. Typical procedure is as follows. 0.20 g of catalyst particles sieved to 250 – 500 μm was placed in the center of a glass tube (ID: 8 mm). The catalyst was pretreated at 250 °C for 1 h in H_2 flow (30 mL/min). Liquid anisole was fed at a rate of 2.29 μL/min (0.020 mmol/min), vaporized at 200 °C, and mixed with H_2 to form anisole/H_2 reactant feed. The anisole concentration was 1.0% and the total flow rate was 48 mL/min. The GHSV and *W*/*F* were 14.4 $L/g_{cat}{\cdot}h$ and 167 $g_{cat}{\cdot}h/mol_{anisole}$, respectively. Then, the catalyst was contacted with the reactant feed at 250 °C to start the reaction. Unreacted anisole and liquid products in effluent gas were collected with ethyl acetate solvent (10 mL) at ice bath temperature every 0.5 h and the obtained solution was analyzed on a SHIMADZU GC-2025 gas chromatograph equipped with a flame ionization detector and a Phenomenex ZB-1 capillary column (30 m × 0.25 mm × 0.25 μm). Products were identified on the basis of mass fragmentation profiles using a SHIMADZU GCMS-QP2010SE gas chromatograph-mass spectrometer. Catalytic reactions were performed multiple times under the same conditions, and the errors in the conversion of anisole and product yields were within ±5%.

3. Results and Discussion

3.1. Structure of Supported CoO_x Samples

Loading amount of cobalt was determined to be 10 ± 0.1 wt% for all the supported CoO_x samples by ICP-AES. XRD patterns of supported CoO_x samples synthesized by heating at 300 °C in He flow are shown in Figure 1. Cobalt species was present in the form of Co_3O_4 (JCPDS 43-1003) on most of the supports. No clear diffraction line was observed for CoO_x/SiO_2, and cobalt species were assumed to be present in highly dispersed state forming cobalt silicate.[10,35,36] For CoO_x/AC, a weak and broad diffraction line of CoO (JCPDS 48-1719) was also observed in addition to those of Co_3O_4. Only for CoO_x/Ti_2O_3, diffraction lines of CoO were mainly observed, and those of Co_3O_4 were much less intense. Additionally, a diffraction line of rutile TiO_2 (JCPDS 21-1276) was slightly observed at 27.5°.

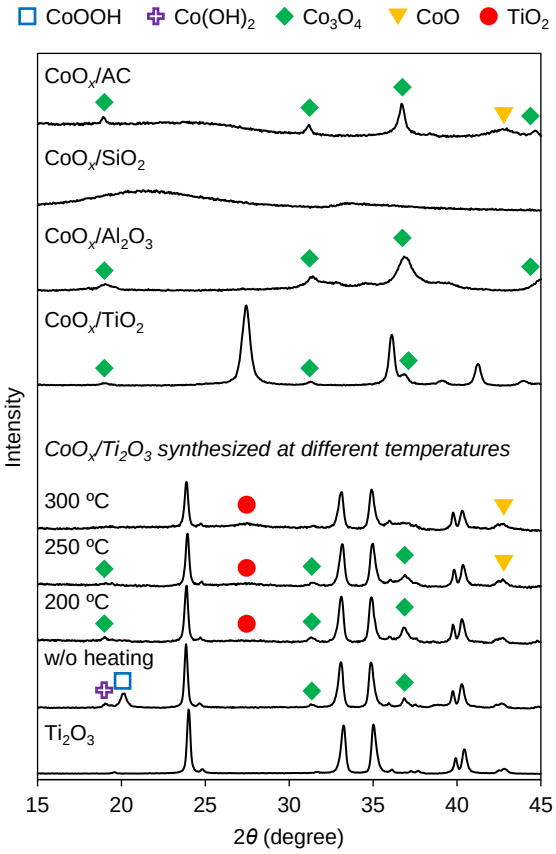

Figure 1 XRD patterns of supported CoO_x samples synthesized by heating in He flow at 300 °C and structural change of CoO_x/Ti_2O_3 upon heating in He flow at different temperatures.

A series of CoO_x/Ti_2O_3 samples were synthesized by heating in He flow at different temperatures, and the structural changes were investigated by XRD (Figure 1). Without heating, cobalt species existed as $Co(OH)_2$ (JCPDS 30-0443) and CoOOH (JCPDS 73-1213), in addition to Co_3O_4. Upon heating at 200 ºC, $Co(OH)_2$ and CoOOH disappeared, and instead diffraction lines for Co_3O_4 became intense. A diffraction line of rutile TiO_2 was also slightly observed. By further increasing the temperature, the intensity of the diffraction lines for Co_3O_4 decreased and that for CoO increased. Simultaneously, the intensity of the diffraction lines for Ti_2O_3 decreased and that for TiO_2 increased (Figure 2). These relevant changes indicated that Co_3O_4 was reduced to CoO, and Ti_2O_3

was partially oxidized to TiO_2. Such oxidation of Ti_2O_3 was also observed as the decrease of Ti^{3+} species and the increase of Ti^{4+} species in Ti 2p X-ray photoelectron spectra (Figure S3a). Therefore, it is considered that Ti_2O_3 acted as reductant to reduce Co_3O_4 to CoO (eq. 1).

$$Co_3O_4 + Ti_2O_3 \rightarrow 3CoO + 2TiO_2 \qquad \text{(eq. 1)}$$

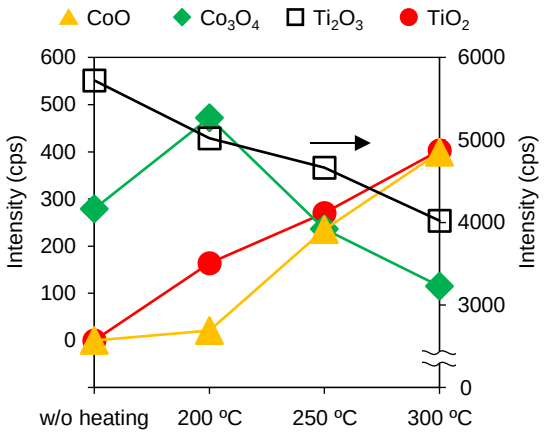

Figure 2 Variation curve for diffraction intensity of CoO ($2\theta = 42.5°$), Co_3O_4 ($2\theta = 31.3°$), Ti_2O_3 ($2\theta = 23.9°$), and TiO_2 ($2\theta = 27.5°$).

Figure 3 shows SEM images of Ti_2O_3 and CoO_x/Ti_2O_3. Ti_2O_3 had smooth particles with the size of ~100 nm. On the other hand, for CoO_x/Ti_2O_3, small CoO_x particles of 20 – 30 nm were observed to be supported on Ti_2O_3 particles. Such small particles were also seen in TEM image of CoO_x/Ti_2O_3_Reduced, which was prepared by reducing CoO_x/Ti_2O_3 with H_2 for catalytic reaction (Figure S4a). CoO_x/TiO_2_Reduced, which was also reduced with H_2, showed much smaller fine particles of cobalt species of less than 10 nm (Figure S4b).

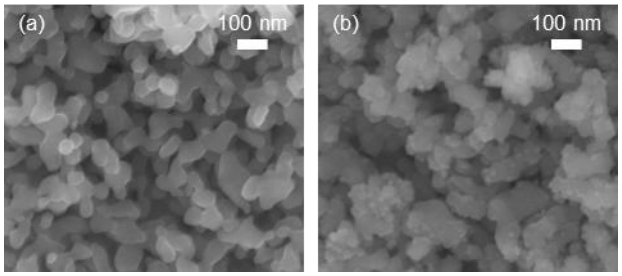

Figure 3 SEM images of (a) Ti_2O_3 and (b) CoO_x/Ti_2O_3.

Reducibility of the unsupported Co_3O_4 and supported CoO_x samples were investigated by H_2-TPR (Figure 4). Unsupported commercial Co_3O_4 (FUJIFILM Wako Pure Chemical) showed a single peak of H_2 consumption at 470 ºC. The average valence of cobalt in Co_3O_4 calculated from this H_2 consumption was +2.65 (Table 1), which was almost consistent with the theoretical value, +2.67. For this reason, it is considered that in the case of unsupported Co_3O_4, once reduction of Co_3O_4 started, the reduction proceeded at once to metallic Co through CoO.

On the other hand, two reduction peaks were observed for the supported CoO_x samples. The low- and high-temperature peaks can be attributed to the reduction of Co_3O_4 to CoO and CoO to Co, respectively.[10,37] CoO_x/Ti_2O_3 showed these two peaks at lower temperature than the others, which suggested that cobalt species on Ti_2O_3 support were more easily reduced. The average valence of cobalt in CoO_x/Ti_2O_3 was +0.99, which was smaller than the theoretical valence of cobalt (+2.0) in CoO, which was the main crystalline phase observed by XRD. The H_2-TPR result for CoO_x/Ti_2O_3 suggested that actually a part of cobalt species existed in the metallic state, which might be generated by the reduction of CoO by Ti_2O_3 (eq. 2).

$$CoO + Ti_2O_3 \rightarrow Co + 2TiO_2 \qquad \text{(eq. 2)}$$

It is considered that such metallic Co was amorphous or existed as fine particles, because no XRD pattern for such species was observed (Figure 1).

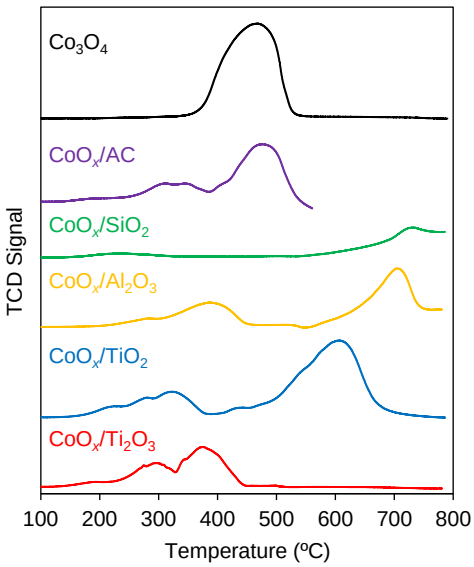

Figure 4 H_2-TPR profiles of supported CoO_x samples and unsupported Co_3O_4.

For the other supported CoO_x samples, the reduction of cobalt species occurred at higher temperature. Particularly, CoO supported on the metal oxide supports (TiO_2, Al_2O_3, and SiO_2) was reduced above 600 ºC. The average valence of cobalt in CoO_x/TiO_2 was +2.51, close to that of Co_3O_4 (+2.67), which was consistent with the observation by XRD. The average valence of cobalt in CoO_x/Al_2O_3 was lower than that expected from the XRD analysis , probably because the reduction of cobalt species did not proceed completely in the H_2-TPR measurement, resulting in the small amount of H_2 consumption. The reduction of cobalt species hardly proceeded on CoO_x/SiO_2. For CoO_x/AC, reduction peaks appeared at 320 and 480 ºC. However, some gases emitted from the AC support during the heating process and overlapped with the detection of H_2 consumption, making it difficult

to quantify the amount of H_2 consumption correctly.

From these results, we concluded that Ti_2O_3 support itself can reduce CoO_x as reductant and retain cobalt species in the low oxidation state under inert atmosphere (Step 1 in Scheme 2). On the other hand, CoO_x on the other supports was not reduced, and thus present as Co_3O_4. The redox interaction between CoO_x and Ti_2O_3 support was a unique property of Ti_2O_3 derived from its strong reducing ability.

Table 1 Specific surface area and reduction properties of supported CoO_x samples.

Sample	S_{BET} [a] ($m^2\ g^{-1}$)	Reduction peak [b] (°C)		V_{bulk} [c] (–)
		Low	High	
CoO_x/Ti_2O_3	18	280	360	0.99
CoO_x/TiO_2	74	320	600	2.51
CoO_x/Al_2O_3	99	380	700	(0.83)
CoO_x/SiO_2	180	n.d.	n.d.	n.d.
CoO_x/AC	1053	320	480	(1.53)
Co_3O_4	n.d.	470		2.65

[a] Specific surface area determined by the BET method.

[b] Reduction peak temperature in H_2-TPR.

[c] Average valence of cobalt in the bulk estimated from the amount of consumed H_2.

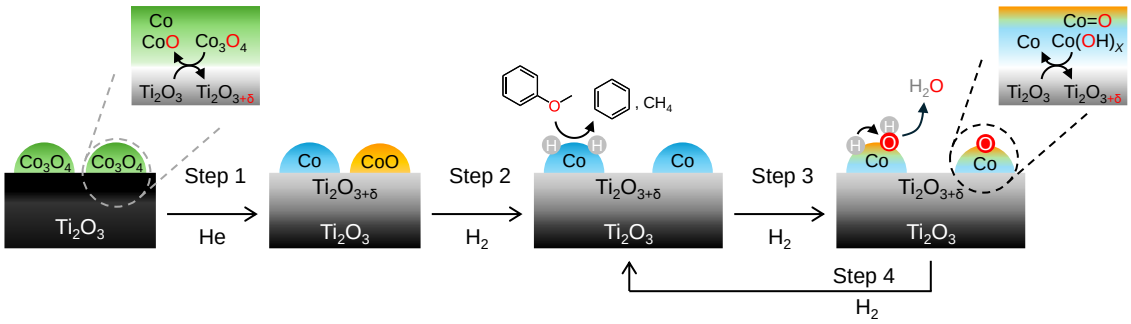

Scheme 2 Structure change of CoO_x/Ti_2O_3 during synthesis and HDO of anisole.

The oxidation state of cobalt near the surface was examined by XPS (Figure 5). CoO_x/Ti_2O_3 showed two broad peaks at around 780 and 795 eV, which are attributed to Co $2p_{3/2}$ and $2p_{1/2}$ peaks, respectively. The spectrum was deconvoluted into several peaks, among which the peaks at 779.6 and 795.1 eV were assignable to $2p_{3/2}$ and $2p_{1/2}$ peaks of Co^{3+}, respectively.[38–40] Those peaks of Co^{2+} appeared at 781.3 and 796.9 eV, respectively. In addition to them, satellite peaks also appeared at around 787 and 802 eV. The average valence of cobalt near the surface was calculated to be 2.61 based on the peak area ratio of the $2p_{3/2}$ peaks (Table 2), which was higher than that of cobalt in the bulk, 0.99 (Table 1). This is due to oxidation of cobalt near the surface when the sample was exposed and stored in air. CoO_x/TiO_2 showed a spectrum similar to that of CoO_x/Ti_2O_3, and the average valence of surface cobalt was almost the same between these two samples. For CoO_x/TiO_2, the average valences of cobalt in the bulk and near the surface were almost the same, indicating that oxidation state of cobalt was uniform in whole the CoO_x particle.

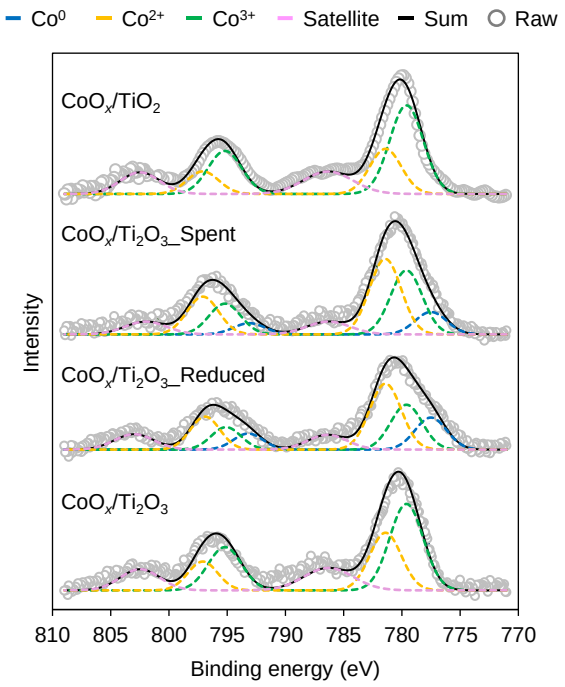

Figure 5 Co 2p X-ray photoelectron spectra of CoO_x/Ti_2O_3 samples and CoO_x/TiO_2. CoO_x/Ti_2O_3_Recuded and CoO_x/Ti_2O_3_Spent were CoO_x/Ti_2O_3 after treatment with H_2 at 250 ºC and after used in the HDO reaction shown in Figure 10, respectively.

Table 2 Proportion of Co^0, Co^{2+}, and Co^{3+} and average valence for CoO_x samples estimated by XPS.

Sample	Proportion [a] (%)			V_{surf} [b]
	Co^0	Co^{2+}	Co^{3+}	(–)
CoO_x/Ti_2O_3	0	39	61	2.61
CoO_x/Ti_2O_3_Reduced	22	47	31	1.87
CoO_x/Ti_2O_3_Spent	11	48	41	2.19
CoO_x/TiO_2	0	32	68	2.68

[a] Proportion of Co $2p_{3/2}$ peak area for Co^0, Co^{2+}, and Co^{3+} species.

[b] Average valence of surface cobalt estimated from the proportion of Co $2p_{3/2}$ peak area.

306 ### 3.2. Hydrodeoxygenation of Anisole over Supported CoO_x Catalysts.

307 Results for HDO of anisole over supported CoO_x catalysts are shown in Figure 6. CoO_x/Ti_2O_3
308 showed the highest activity with high selectivity to benzene. CoO_x/TiO_2 and CoO_x/AC showed the
309 second highest activity, while CoO_x/Al_2O_3, and CoO_x/SiO_2 showed almost no activity. In addition to
310 benzene, several products such as cyclohexane, methoxycyclohexane, and phenol were produced as
311 by-products (Table 3). There were no unidentified by-products (Figure S5). For these catalysts, the
312 carbon balance was ~90% or higher. From these results, it is considered that the difference in the
313 catalytic performance was due to the difference in the physical and chemical properties of the
314 catalysts.

315 Generally, the larger specific surface area leads to higher activity. However, for the series of
316 supported CoO_x catalysts tested in this study, no clear correlation was observed between the specific
317 surface area and catalytic activity (Table 1). Also, a catalyst with smaller particle size of cobalt species
318 would show higher activity, but no such trend was observed between CoO_x/Ti_2O_3 and CoO_x/TiO_2
319 (Figure S4). Rather, a correlation was observed between the oxidation state of cobalt and catalytic
320 activity; CoO_x/Ti_2O_3, which contained metallic Co, showed the highest activity, while CoO_x/Al_2O_3,
321 and CoO_x/SiO_2, on which CoO_x was less susceptible to reduction, showed the lowest activity.

322 MoO_x/ZrO_2, which has been reported to show the high activity for HDO of anisole at
323 relatively low temperatures and atmospheric pressure of H_2, was also used for comparison.[34]
324 MoO_x/ZrO_2 was active only at 300 ºC or higher (Figure 6) and gave a large amount of by-products
325 such as toluene and cresol (Table S2). This is because side reactions such as intramolecular

methylation and/or transmethylation were more likely to occur over acid sites of the catalyst at high temperature. To selectively promote the HDO of anisole to benzene, low temperature reaction using a highly active catalyst is desired. In fact, when the reaction was conducted at higher temperatures using CoO_x/Ti_2O_3, the selectivity to benzene was significantly decreased, while the conversion of anisole was increased (Figure S6). Compared with the results reported so far on the vapor-phase HDO of anisole, CoO_x/Ti_2O_3 showed relatively high conversion and high selectivity to benzene under mild conditions such as less than 300 °C and 0.1 MPa of H_2 pressure (Table S3).

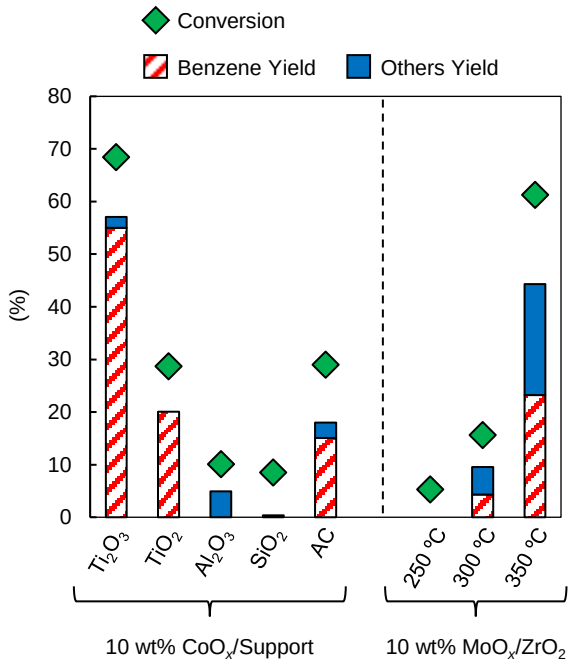

Figure 6 Hydrodeoxygenation of anisole over supported CoO_x catalysts at 250 ºC or MoO_x/ZrO_2 catalyst at 250 – 350 ºC.

Pretreatment conditions: H_2 flow (30 mL min^{-1}) at 250 ºC for 1 h. Reaction conditions: Catalyst, 0.20 g; Anisole, 0.020 mmol min^{-1}; Total flow rate (H_2 balance), 48 mL min^{-1}; Temperature, 250 ºC for supported CoO_x catalysts or 250 – 350 ºC for MoO_x/ZrO_2 catalyst; Time on stream, 1 h.

Table 3 Detailed results for hydrodeoxygenation of anisole over supported CoO_x catalysts at 250 ºC.

	CoO_x/Support				
	Ti_2O_3	TiO_2	Al_2O_3	SiO_2	AC
Conversion (%)	68.5	28.7	10.1	8.5	29.0
Products yield (%)					
Benzene	55.0	20.1	0.0	0.3	15.1
Cyclohexane	1.1	0.0	0.0	0.0	0.6
Methoxycyclohexane	0.0	0.0	0.0	0.0	2.3
Phenol	0.0	0.0	3.4	0.0	0.0
Cresol	0.0	0.0	1.1	0.0	0.0
Toluene	1.0	0.0	0.0	0.0	0.0
Methylanisole	0.0	0.0	0.4	0.0	0.0
Dimethylanisole	0.0	0.0	0.6	0.0	0.0

3.3. Support Effect on Co Speciation and Catalytic Properties of Supported CoO_x

To emphasize the support effect on the oxidation state of the cobalt species and on the catalytic performance, CoO_x/Ti_2O_3 and CoO_x/TiO_2 were pretreated under different conditions and used for the HDO of anisole (Figure 7). Regardless of the pretreatment conditions, CoO_x/Ti_2O_3 always showed higher activity than CoO_x/TiO_2, when they were pretreated under the same conditions. Commonly to both catalysts, the conversion of anisole and the yield of benzene increased with increase of the temperature for reduction pretreatment with H_2. In particular, the activity of CoO_x/TiO_2 was significantly increased by increasing the reduction temperature. Increasing the reduction temperature from 350 to 450 °C had no significant effect on the catalytic performance of CoO_x/Ti_2O_3. When pretreated with N_2 instead of H_2 at 250 °C, CoO_x/Ti_2O_3 showed only slight decrease in the activity, while CoO_x/TiO_2 was no longer active for the reaction. These results indicated that CoO_x was

already reduced by Ti_2O_3 during the synthesis by heating in He flow at 300 °C, providing catalytically active state.

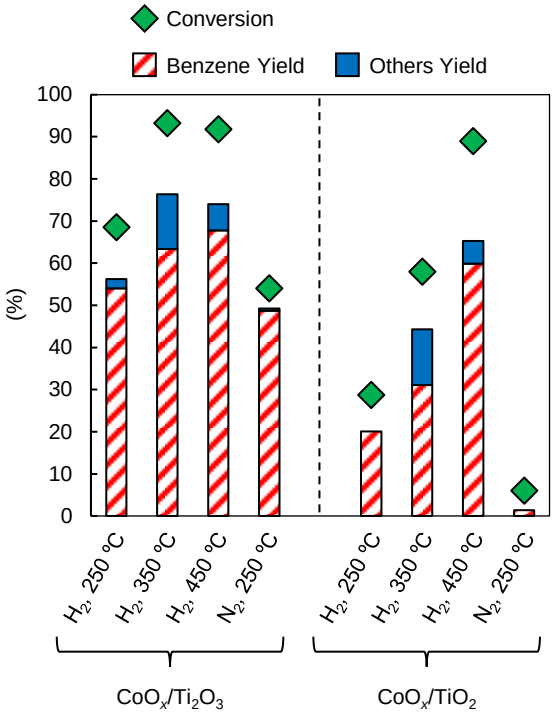

Figure 7 Effect of pretreatment conditions on the catalytic performance of CoO_x/Ti_2O_3 and CoO_x/TiO_2 for hydrodeoxygenation of anisole.

Pretreatment conditions: N_2 or H_2 flow (30 mL min^{-1}) at 250 – 450 ºC for 1 h. Reaction conditions: CoO_x/Ti_2O_3 or CoO_x/TiO_2, 0.20 g; Anisole, 0.20 mmol min^{-1}; Total flow rate (H_2 balance), 48 mL min^{-1}; Temperature, 250 ºC; TOS, 1 h.

Figure 8 shows XRD patterns of the samples pretreated under different conditions, which were the same as those in Figure 7. For CoO_x/Ti_2O_3, a part of CoO was reduced to metallic Co by the reduction with H_2 at 250 °C, and only metallic Co existed at 350 °C or higher. The crystallite size of

metallic Co for the sample reduced at 250 °C (identical to CoO_x/Ti_2O_3_Reduced) was estimated to be 34 nm by the Scherrer equation, which was in good agreement with the particle sizes observed by TEM (Figure S4a). On the other hand, for CoO_x/TiO_2, only CoO was produced by the reduction at 250 °C, and metallic Co formed in the reduction at 350 °C or higher. For CoO_x/Ti_2O_3, the diffraction line intensity of metallic Co increased with increase of the reduction temperature and simultaneously, that of Ti_2O_3 decreased (Figure S7a). This indicated that redox reaction occurred between Ti_2O_3 and CoO_x, as in the case of heating in He flow (Figure 2). In other words, even in the reductive atmosphere with H_2, CoO_x was reduced not only by H_2 but also by Ti_2O_3. For CoO_x/TiO_2, no such redox reaction occurred between cobalt species and the support (Figure S7b).

The average valence of cobalt in CoO_x/Ti_2O_3 and CoO_x/TiO_2 pretreated with H_2 or N_2 at 250 and 350 °C was estimated by the H_2-TPR, and the relationship between the average valence of cobalt and the activity was examined (Figure S8). A clear correlation was found between the decrease in the average valence of cobalt and the increase in the activity. Therefore, it is reasonable to conclude that the difference in the activity of the supported CoO_x catalysts was due to the difference in the oxidation state of cobalt in the CoO_x on each support and that the highest activity of CoO_x/Ti_2O_3 was due to the reduction of cobalt species by Ti_2O_3 with the strong reducing ability.

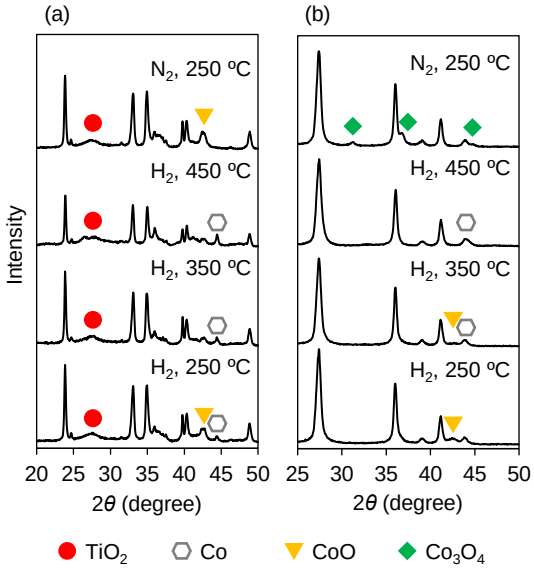

Figure 8 XRD patterns of (a) CoO_x/Ti_2O_3 and (b) CoO_x/TiO_2 after treatment with H_2 or N_2 at 250 – 450 ºC.

As shown above, the activity increased as the valence of cobalt decreased. Similar tendency was found by other research groups in the HDO reactions using cobalt catalysts and it was proposed that the reason for such tendency was that metallic Co had the ability to adsorb and activate H_2.[7,11,20] To confirm whether the same phenomenon occurred with our catalysts, H_2-TPD measurements were performed on CoO_x/Ti_2O_3 and CoO_x/TiO_2. As Figure 9 clearly shows, desorption of H_2 was observed at ~400 °C for CoO_x/Ti_2O_3, while no H_2 was desorbed from CoO_x/TiO_2, meaning that no H_2 was adsorbed on CoO_x/TiO_2. It is presumable that effective adsorption and activation of H_2 on metallic Co brought about the high catalytic activity of CoO_x/Ti_2O_3. In fact, when HDO of anisole was performed using CoO_x/Ti_2O_3 and CoO_x/TiO_2 at different H_2 partial pressures, CoO_x/Ti_2O_3 had lower dependence on the H_2 partial pressure than CoO_x/TiO_2 did (Figure S9). Ti_2O_3 support was effective for facilitating the reduction of CoO_x and maintaining metallic Co to adsorb and activate H_2 during the HDO of anisole.

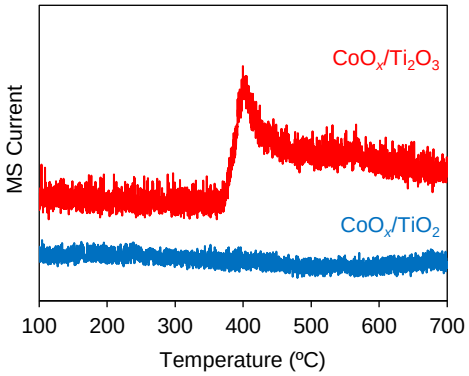

Figure 9 H_2-TPD profiles of CoO_x/Ti_2O_3 and CoO_x/TiO_2.

Influence of the synthesis temperature on the state of cobalt species and catalytic performance of CoO_x/Ti_2O_3 was examined. By increasing the temperature for heating CoO_x/Ti_2O_3 in He flow from 300 °C to 400 or 500 °C, the reduction of cobalt species proceeded more deeply, and CoO was reduced to metallic Co according to eq. 2 (Figure S10a). However, the catalytic activity decreased with increasing the synthesis temperature (Figure S10b). As the dispersion of metallic Co estimated from CO adsorption measurement decreased with increasing synthesis temperature, the activity decrease was due to the significant particle aggregation of cobalt species that occurred at the high temperature. From these results, it was determined that 300 °C was the optimal synthesis temperature for CoO_x/Ti_2O_3.

Influence of cobalt loading was also investigated on CoO_x/Ti_2O_3. In addition to the standard loading of 10 wt%, which has been described so far, the loadings of 2.5, 5, and 20 wt% were also investigated. Up to 10 wt% loading, CoO was the predominant cobalt species (Figure S11a), indicating that most or all of Co_3O_4 was reduced to CoO by Ti_2O_3 (eq. 1). Meanwhile, Co_3O_4 was

present significantly for 20 wt% loading. Presumably, for 20 wt% loading, a part of Co_3O_4 particles did not contact with Ti_2O_3, and therefore such Co_3O_4 particles remained without being reduced. Up to 10 wt% loading, the catalytic activity and benzene yield increased with the loading, but the benzene yield did not increase upon further increasing the cobalt loading to 20 wt%, (Figure S11b). This is because, for 20 wt% loading, the insufficiently reduced cobalt species had only poor activity for the HDO reaction.

3.4. Effect of Ti_2O_3 Support on Stability of Co Species.

The stability and life of catalysts are important catalytic performance, hence, those of CoO_x/Ti_2O_3 and CoO_x/TiO_2 for the HDO of anisole were evaluated (Figure 10). For CoO_x/Ti_2O_3, the conversion of anisole dropped from 70% to 60% in the first 3 h, but then decreased only slowly to ~50% until 48 h. Total yield of products including benzene and cyclohexane also decreased slowly. On the other hand, for CoO_x/TiO_2, the conversion of anisole dropped from 60% to 30% in just 2 h and continued to decrease to 20% by 25 h. These results indicated that CoO_x/Ti_2O_3 was more stable against deactivation, leading to the longer catalyst life.

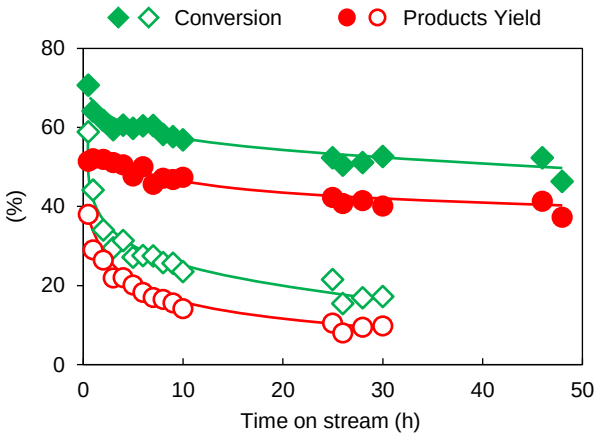

Figure 10 Catalyst life of CoO_x/Ti_2O_3 (filled) and CoO_x/TiO_2 (blank) for HDO of anisole. Pretreatment conditions: H_2 flow (30 mL min^{-1}) at 250 ºC for 1 h. Reaction conditions: CoO_x/Ti_2O_3 or CoO_x/TiO_2, 0.40 g; Anisole, 0.020 mmol min^{-1}; Total flow rate (H_2 balance), 48 mL min^{-1}; Temperature, 200 ºC.

To understand the cause of deactivation, the structure of CoO_x/Ti_2O_3 was examined by XRD after the reaction, but no clear difference was observed between the sample after the pretreatment with H_2 and the spent catalyst (Figure S12). There was no clear change in the particle size of cobalt species for CoO_x/Ti_2O_3 and CoO_x/TiO_2, either (Figure S4). Furthermore, almost no or only a slight organic compound was deposited on these two spent catalysts, implying that the deactivation was not caused by the deposition of organic compounds (Figure S13). Then, the oxidation state of cobalt in the spent CoO_x/Ti_2O_3 was analyzed by XPS (Figure 5 and Table 2). Compared with the sample after the pretreatment with H_2, the proportion of Co^0 decreased, while that of Co^{3+} increased after the reaction. Therefore, the oxidation of cobalt during the reaction was assumed to cause the deactivation. To demonstrate this assumption, the supply of anisole was stopped with H_2 flow continued in the

middle of the reaction using CoO_x/Ti_2O_3 and CoO_x/TiO_2. By this operation, the spent catalysts would be reduced in H_2 flow. Then, the supply of anisole was resumed, and the activity was evaluated again (Figure S14). The results of repeating this procedure showed that the activity was restored repeatedly by the reduction with H_2, demonstrating that the oxidation of cobalt species was the cause of the deactivation. Probably, oxygen derived from anisole oxidized the cobalt species as oxo or hydroxide species (Step 3 in Scheme 2).

The slow deactivation and long catalyst life of CoO_x/Ti_2O_3 implied that the reduction of oxidized cobalt species during the reaction was likely to occur on this catalyst. Indeed, the reduction of CoO_x proceeded on CoO_x/Ti_2O_3 at low temperature in H_2 atmosphere (Figures 4 and 8). Under these conditions, not only H_2 but also Ti_2O_3 support was responsible for the reduction of the oxidized cobalt species CoO_x. This reductive function was unique to Ti_2O_3, which contributed to the enhanced catalytic activity at low temperature and extended catalyst life for the HDO reaction.

3.5. Role of Ti_2O_3 Support in HDO Reaction of Anisole.

From the results so far, it was found that the redox reaction occurred between CoO_x and Ti_2O_3, and Ti_2O_3 had the ability to reduce CoO_x. The reducing property of Ti_2O_3 not only functioned in the synthesis in inert atmosphere (Step 1 in Scheme 2), but also played a vital role in the reduction of CoO_x in H_2 atmosphere (Step 2). CoO_x was reduced to the metallic state on Ti_2O_3 by the combined reducing action of H_2 and Ti_2O_3, whereas CoO_x was mainly reduced only to CoO on the other supports. H_2 adsorbed and activated on the metallic Co reductively cleaved the C-O bonds of anisole, and the

HDO reaction proceeded. The oxidation of cobalt species caused by oxygen remaining on the catalyst caused the deactivation of the supported CoO_x catalysts (Step 3). Over CoO_x/Ti_2O_3 with the redox interaction, CoO_x was reduced by not only H_2 but also Ti_2O_3, which made it easier for the oxidized cobalt species to be reduced (Step 4). Maintaining the cobalt species in the metallic state in this manner helped maintain high catalytic activity over time.

Conclusions

In this study, we demonstrated the redox interaction between cobalt species and Ti_2O_3 support. CoO_x supported on Ti_2O_3 was reduced to metallic state by Ti_2O_3 in inert atmosphere. Metallic Co had the ability to activate H_2 and thus, CoO_x/Ti_2O_3 showed the highest activity for the HDO of anisole among the supported CoO_x catalysts. CoO_x/Ti_2O_3 gave 69% conversion of anisole and 79% selectivity to benzene at 250 °C and atmospheric pressure of H_2. Partial oxidation of cobalt species occurred during the HDO reaction and caused the deactivation of the supported CoO_x catalysts. Over CoO_x/Ti_2O_3, the oxidized cobalt species were reduced by Ti_2O_3 support as well as H_2, which facilitated keeping cobalt in the low oxidation state and maintained the high activity for a long period without serious deactivation.

Supporting Information

Detailed data on product distribution, influence of reaction temperature, H_2 pressure dependence, catalyst regeneration and so on are available in Supporting Information.

Acknowledgements

This research was supported by JSPS KAKENHI Grant Number JP21K14457 and JP23K04493, JST SPRING Grant Number JPMJSP2119, and Takahashi Industrial and Economic Research Foundation. A part of this work was conducted at Laboratory of XPS analysis, Joint-use facilities, Hokkaido university. We thank the Open Facility, Global Facility Center, Creative Research Institution, Hokkaido University for allowing us to conduct the analysis with ICP-AES and providing insight and expertise that greatly assisted the research.

References

(1) Furimsky, E. Catalytic hydrodeoxygenation. *Applied Catalysis A: General* **2000**, *199* (2), 147-190. https://doi.org/10.1016/S0926-860X(99)00555-4.

(2) Prabhudesai, V. S.; Gurrala, L.; Vinu, R. Catalytic Hydrodeoxygenation of Lignin-Derived Oxygenates: Catalysis, Mechanism, and Effect of Process Conditions. *Energy Fuels* **2022**, *36* (3), 1155–1188. https://doi.org/10.1021/acs.energyfuels.1c02640.

(3) Sreenavya, A.; Aswin, P.; Ganesh, V.; Venkatesha, N. J.; Sakthivel, A. Facile water-free synthesis of noble metal-containing hydrotalcites-derived materials and their application for hydrotreatment of anisole. *Materials Today Sustainability* **2022**, *18*. https://doi.org/10.1016/j.mtsust.2022.100153.

(4) Dutta, S.; Shumeiko, B.; Aubrecht, J.; Karásková, K.; Fridrichová, D.; Pacultová, K.; Hlinčík, T.; Kubička, D. Evaluation of anisole hydrodeoxygenation reaction pathways over a Ni/Al_2O_3 Catalyst. *Journal of Catalysis* **2024**, *435*. https://doi.org/10.1016/j.jcat.2024.115553.

(5) Jin, W.; Pastor-Pérez, L.; Shen, D. K.; Sepúlveda-Escribano, A.; Gu, S.; Ramirez Reina, T. Catalytic Upgrading of Biomass Model Compounds: Novel Approaches and Lessons Learnt from Traditional Hydrodeoxygenation – a Review. *ChemCatChem* **2019**, *11* (3). https://doi.org/10.1002/cctc.201801722.

(6) Reina, A.; Carmona-Chávez, R.; Pulido-Díaz, I. T.; Martínez, D.; Salas-Martin, K. P.;

Guerrero-Ríos, I. Silica-Supported 1st Row Transition Metal (Nano) Catalysts: Synthetic and Catalytic Insight. *ChemCatChem* **2023**, *15* (11). https://doi.org/10.1002/cctc.202300285.

(7) Mochizuki, T.; Chen, S. Y.; Toba, M.; Yoshimura, Y. Deoxygenation of guaiacol and woody tar over reduced catalysts. *Applied Catalysis B:Environmental* **2014**, *146*, 237–243. https://doi.org/10.1016/j.apcatb.2013.05.040.

(8) Infantes-Molina, A.; Gralberg, E.; Cecilia, J. A.; Finocchio, E.; Rodríguez-Castellón, E. Nickel and cobalt phosphides as effective catalysts for oxygen removal of dibenzofuran: role of contact time, hydrogen pressure and hydrogen/feed molar ratio. *RSC Catalysis Science & Technology* **2015**, *5* (6), 3403–3415. https://doi.org/10.1039/c5cy00282f.

(9) Srifa, A.; Viriya-empikul, N.; Assabumrungrat, S.; Faungnawakij, K. Catalytic behaviors of Ni/γ-Al_2O_3 and Co/γ-Al_2O_3 during the hydrodeoxygenation of palm oil. *RSC Catalysis Science & Technology* **2015**, *5* (7), 3693–3705. https://doi.org/10.1039/c5cy00425j.

(10) Yang, Y.; Lv, G.; Deng, L.; Lu, B.; Li, J.; Zhang, J.; Shi, J.; Du, S. Renewable aromatic production through hydrodeoxygenation of model bio-oil over mesoporous Ni/SBA-15 and Co/SBA-15. *Microporous and Mesoporous Materials* **2017**, *250* (15), 47–54. https://doi.org/10.1016/j.micromeso.2017.05.022.

(11) Liu, X.; Jia, W.; Xu, G.; Zhang, Y.; Fu, Y. Selective Hydrodeoxygenation of Lignin-Derived Phenols to Cyclohexanols over Co-Based Catalysts. *ACS Sustainable Chem. Eng.* **2017**, *5* (10), 8594–8601. https://doi.org/10.1021/acssuschemeng.7b01047.

(12) Wu, G.; Zhang, N.; Dai, W.; Guan, N.; Li, L. Construction of Bifunctional Co/H-ZSM-5 Catalysts for the Hydrodeoxygenation of Stearic Acid to Diesel-Range Alkanes. *ChemSusChem* **2018**, *11* (13), 2179-2188. https://doi.org/10.1002/cssc.201800670.

(13) Xu, Q.; Shi, Y.; Yang, L.; Fan, G.; Li, F. The promotional effect of surface Ru decoration on the catalytic performance of Co-based nanocatalysts for guaiacol hydrodeoxygenation. *Molecular Catalysis* **2020**, *497*. https://doi.org/10.1016/j.mcat.2020.111224.

(14) Kim, H.; Lim, Y. H.; Park, J. H.; Ha, J. M.; Kim, D. H. Hydrodeoxygenation of guaiacol over physically mixed Co/TiO_2 and WO_3/TiO_2 catalysts. *RSC Green Chemistry* **2024**, *26* (5), 2692–2704. https://doi.org/10.1039/d3gc04400a.

(15) Hongkailers, S.; Pattiya, A.; Hinchiranan, N. Hydrodeoxygenation of Oxygenates Derived from Biomass Pyrolysis Using Titanium Dioxide-Supported Cobalt Catalysts. *Molecules* **2023**, *28* (22). https://doi.org/10.3390/molecules28227468.

(16) Zhu, Z.; Zhang, C.; Zhou, P.; Han, B.; Zhang, Z.; Liu, B. Carbon-supported Co/Co_3O_4 hybrid catalyst: an efficient non-noble metal catalyst for the hydrodeoxygenation of vanillin. *RSC Catalysis Science & Technology* **2023**, *13* (21), 6233–6237. https://doi.org/10.1039/d3cy00971h.

(17) Ranga, C.; Alexiadis, V. I.; Lauwaert, J.; Lødeng, R.; Thybaut, J. W. Effect of Co incorporation and support selection on deoxygenation selectivity and stability of (Co)Mo catalysts in anisole HDO. *Applied Catalysis A General* **2019**, *571 (5)*, 61–70. https://doi.org/10.1016/j.apcata.2018.12.004.

(18) Liu, M.; Zhang, J.; Zheng, L.; Fan, G.; Yang, L.; Li, F. Significant Promotion of Surface Oxygen Vacancies on Bimetallic CoNi Nanocatalysts for Hydrodeoxygenation of Biomass-derived Vanillin to Produce Methylcyclohexanol. *ACS Sustainable Chem. Eng.* **2020**, *8* (15), 6075–6089. https://doi.org/10.1021/acssuschemeng.0c01015.

(19) Ballesteros-Plata, D.; Barroso-Martín, I.; Medina Cervantes, J. A.; Maciel, C.; Huirache-Acuña, R.; Rodríguez-Castellón, E.; Infantes-Molina, A. Bimetallic Niobium-Based Catalysts Supported on SBA-15 for Hydrodeoxygenation of Anisole. *Ind. Eng. Chem. Res.* **2021**, *60* (51), 18831–18840. https://doi.org/10.1021/acs.iecr.1c02799.

(20) Geng, Y.; Li, H. Hydrogen Spillover-Enhanced Heterogeneously Catalyzed Hydrodeoxygenation for Biomass Upgrading. *ChemSusChem* **2022**, *15* (8). https://doi.org/10.1002/cssc.202102495.

(21) Schanke, D.; Hilmen, A. M.; Bergene, E.; Kinnari, K.; Rytter, E.; Ådnanes, E.; Holmen, A. Reoxidation and Deactivation of Supported Cobalt Fischer-Tropsch Catalysts. *Energy Fuels* **1996**, *10* (4), 867–872. https://doi.org/10.1021/ef950197u.

(22) Ouedraogo, A. S.; Bhoi, P. R. Recent progress of metals supported catalysts for hydrodeoxygenation of biomass derived pyrolysis oil. *Journal of Cleaner Production* **2020**, *253* (20). https://doi.org/10.1016/j.jclepro.2020.119957.

(23) Lindfors, C.; Mäki-Arvela, P.; Paturi, P.; Aho, A.; Eränen, K.; Hemming, J.; Peurla, M.; Kubička, D.; Simakova, I. L.; Murzin, D. Y. Hydrodeoxygenation of Isoeugenol over Ni- and Co-Supported Catalysts. *ACS Sustainable Chem. Eng.* **2019**, *7* (17), 14545–14560. https://doi.org/10.1021/acssuschemeng.9b02108.

(24) Shit, S. C.; Koley, P.; Joseph, B.; Marini, C.; Nakka, L.; Tardio, J.; Mondal, J. Porous Organic Polymer-Driven Evolution of High-Performance Cobalt Phosphide Hybrid Nanosheets as Vanillin Hydrodeoxygenation Catalyst. *ACS Appl. Mater. Interfaces* **2019**, *11* (27), 24140–24153. https://doi.org/10.1021/acsami.9b06789.

(25) Yu, H.; Xu, Y.; Zhang, M.; Zhang, L.; Wu, W.; Huang, K. Magnetically-separable cobalt catalyst embedded in metal nitrate-promoted hierarchically porous N-doped carbon nanospheres for hydrodeoxygenation of lignin-derived species. *Fuel* **2023**, *331* (2). https://doi.org/10.1016/j.fuel.2022.125917.

(26) Lee, J.; Burt, S. P.; Carrero, C. A.; Alba-Rubio, A. C.; Ro, I.; O'Neill, B. J.; Kim, H. J.; Jackson, D. H. K.; Kuech, T. F.; Hermans, I.; Dumesic, J. A.; Huber, G. W. Stabilizing cobalt catalysts

for aqueous-phase reactions by strong metal-support interaction. *Journal of Catalysis* **2015**, *330*, 19–27. https://doi.org/10.1016/j.jcat.2015.07.003.

(27) Li, Y.; Zhu, Y.; Wang, M.; Zhao, M.; Xue, J.; Chen, J.; Wu, T.; Chambers, S. A. Recent Progress on Titanium Sesquioxide: Fabrication, Properties, and Applications. *Advanced Functional Materials* **2022**, *32* (33). https://doi.org/10.1002/adfm.202203491.

(28) Kumar, A.; Barbhuiya, N. H.; Singh, S. P. Magnéli phase titanium sub-oxides synthesis, fabrication and its application for environmental remediation: Current status and prospect. *Chemosphere* **2022**, *307* (2). https://doi.org/10.1016/j.chemosphere.2022.135878.

(29) Wu, X.; Wang, H.; Wang, Y. A Review: Synthesis and Applications of Titanium Sub-Oxides. *Materials* **2023**, *16* (21). https://doi.org/10.3390/ma16216874.

(30) Baktash, E.; Capitolis, J.; Tinat, L.; Larquet, C.; Chan Chang, T. H. C.; Gallet, J. J.; Bournel, F.; Sanchez, C.; Carenco, S.; Portehault, D. Different Reactivity of Rutile and Anatase TiO_2 Nanoparticles: Synthesis and Surface States of Nanoparticles of Mixed-Valence Magnéli Oxides. *Chemistry A European Journal* **2019**, *25* (47), 11114–11120. https://doi.org/10.1002/chem.201901592.

(31) Nagao, M.; Misu, S.; Hirayama, J.; Otomo, R.; Kamiya, Y. Magneli-Phase Titanium Suboxide Nanocrystals as Highly Active Catalysts for Selective Acetalization of Furfural. *ACS Appl. Mater. Interfaces* **2020**, *12* (2), 2539–2547. https://doi.org/10.1021/acsami.9b19520.

(32) Liu, Z.; Li, J.; Buettner, M.; Ranganathan, R. V.; Uddi, M.; Wang, R. Metal-Support Interactions in CeO_2 -and SiO_2 -Supported Cobalt Catalysts: Effect of Support Morphology, Reducibility, and Interfacial Configuration. *ACS Appl. Mater. Interfaces* **2019**, *11* (18), 17035–17049. https://doi.org/10.1021/acsami.9b02455.

(33) Qin, Z.; Wang, X.; Dong, L.; Su, T.; Li, B.; Zhou, Y.; Jiang, Y.; Luo, X.; Ji, H. CO_2 methanation on Co/TiO_2 catalyst: Effects of Y on the support. *Chemical Engineering Science* **2019**, *210* (31). https://doi.org/10.1016/j.ces.2019.115245.

(34) Shetty, M.; Murugappan, K.; Green, W. H.; Román-Leshkov, Y. Structural Properties and Reactivity Trends of Molybdenum Oxide Catalysts Supported on Zirconia for the Hydrodeoxygenation of Anisole. *ACS Sustainable Chem. Eng.* **2017**, *5* (6), 5293–5301. https://doi.org/10.1021/acssuschemeng.7b00642.

(35) Umegaki, T.; Yan, J. M.; Zhang, X. B.; Shioyama, H.; Kuriyama, N.; Xu, Q. $Co\text{-}SiO_2$ nanosphere-catalyzed hydrolytic dehydrogenation of ammonia borane for chemical hydrogen storage. *Journal of Power Sources* **2010**, *195* (24), 8209–8214. https://doi.org/10.1016/j.jpowsour.2010.07.079.

(36) Zhang, Q.; Chen, C.; Wang, M.; Cai, J.; Xu, J.; Xia, C. Facile preparation of highly-dispersed cobalt-silicon mixed oxide nanosphere and its catalytic application in cyclohexane selective

oxidation. *Nanoscale Research Letters* **2011**, *6* (586). https://doi.org/10.1186/1556-276X-6-586.

(37) Nabaho, D.; Niemantsverdriet, J. W.; Claeys, M.; Van Steen, E. Hydrogen spillover in the Fischer–Tropsch synthesis: An analysis of platinum as a promoter for cobalt–alumina catalysts. *Catalysis Today* **2016**, *261*, 17–27. https://doi.org/10.1016/j.cattod.2015.08.050.

(38) Si, J.; Xiao, S.; Wang, Y.; Zhu, L.; Xia, X.; Huang, Z.; Gao, Y. Sub-nanometer Co_3O_4 clusters anchored on TiO_2 (B) nano-sheets: Pt replaceable Co-catalysts for H_2 evolution. *RSC Nanoscale* **2018**, *10* (5), 2596–2602. https://doi.org/10.1039/c7nr07336d.

(39) Wang, J.; Nie, R.; Xu, L.; Lyu, X.; Lu, X. Catalytic transfer hydrogenation of oleic acid to octadecanol over magnetic recoverable cobalt catalysts. *RSC Green Chemistry* **2019**, *21* (2), 314–320. https://doi.org/10.1039/c8gc03075h.

(40) Wu, L.; Wei, J.; Zhang, Y.; He, Y.; Wang, X.; Guo, H.; Tang, Y.; Tan, L. The selective hydrodeoxygenation of guaiacol to cyclohexanol over cobalt-modified TS-1 catalysts. *Microporous and Mesoporous Materials* **2023**, *348* (15). https://doi.org/10.1016/j.micromeso.2022.112347.

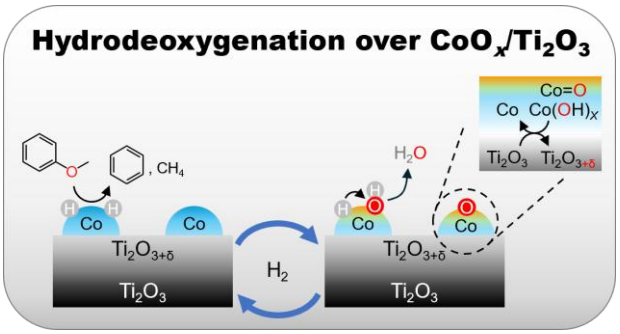
Hydrodeoxygenation over CoO_x/Ti_2O_3
Co=O
Co Co(OH)x
Ti_2O_3 $Ti_2O_{3+\delta}$
, CH_4
H_2O
Co
Co
$Ti_2O_{3+\delta}$
Ti_2O_3
H_2
Co
Co
$Ti_2O_{3+\delta}$
Ti_2O_3

TOC graphic

644 This research developed the highly active catalysts for selective chemical conversion of lignin-
645 derived materials.